# A PROBABILISTIC APPROACH FOR REGISTRATION OF MULTI-MODAL SPATIAL TRANSCRIPTOMICS DATA

*Yu Qiang*[1,2], *Shixu He*[1], *Rengpeng Ding*[1], *Yuxiang Li*[1], *Yong Hou*[1], *Yan Zhou*[1,*], *and Karl Rohr*[2,*]

[1]MGI, BGI-Shenzhen, Shenzhen, 518083, China
[2]Heidelberg University, BioQuant, IPMB, and DKFZ Heidelberg,
Biomedical Computer Vision Group, Im Neuenheimer Feld 267, 69120 Heidelberg, Germany

## ABSTRACT

Observing the spatial characteristics of gene expression by image-based spatial transcriptomics technology allows studying gene activities across different cells and intracellular structures. We introduce a probabilistic approach for the registration and analysis of transcriptome images and immunostaining images. The method is based on particle filters, exploits both intensity information and image features, and takes into account multi-channel information. We applied our approach to two-channel synthetic data as well as real transcriptome images and immunostaining microscopy images of the mouse brain. It turns out that our approach accurately registers the multi-modal images and yields better results than a state-of-the-art method.

***Index Terms*—** Spatial transcriptomics, multi-modal images, registration, probabilistic method

## 1. INTRODUCTION

Spatial transcriptomics (ST) technologies based on next generation sequencing (NGS) systematically generate spatial measurements of gene expression in an entire tissue sample, which bridge the gap between spatial information and the whole transcriptome [1]. Advanced spatial transcriptomics platforms, like Stereo-seq [2] or Seq-scope [3], achieve nanoscale resolution, enabling determining subcellular compartmentalization and visualization of RNAs.

However, for current ST technologies with nanoscale resolution it is difficult to accurately associate spots of transcriptome images into specific organelles or cells [1]. The gene expression matrix can be exploited in different ways, for example, to characterize gene expression patterns or to classifiy cell types in the tissue region of interest [4–6]. However, lack of distinct cell boundaries in the gene expression matrix presents a huge challenge for automated analysis. Fast and precise registration of transcriptome images and immunostaining images will facilitate the assignment of expressed genes to specific cells according to enable studying sub-cellular expression pattern.

* Corresponding authors.

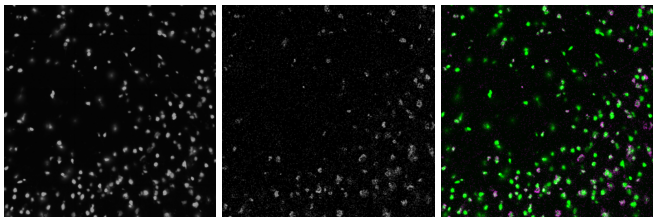

(a) (b) (c)

**Fig. 1**. Registration result of our approach for an image section: (a) Immunostaining image, (b) gene expression matrix image, and (c) overlay of registered images.

Although in situ sequencing and immunostaining are carried out on the same tissue, there are multiple factors that can cause the spatial shifting, due to the sample preparation process and dispersion of RNAs after tissue permeabilization. Manual alignment of two images is time consuming, and only enables partial alignment in most cases [3, 6]. Therefore, methods are needed for efficient and accurate registration of large-scale transcriptome images and immunostaining images with tens of thousands of cells.

In previous work on automatic registration of spatial transcriptomics image data only few methods were introduced. [7] described a method that uses intensity-based and feature-based information. However,the information in the different data channels is treated separately. Improved results can be obtained by jointly exploiting the information in the different image channels. [8] described a method that determines the transformation between the image channels by combining intensity-based and feature-based information. However, the method is computationally expensive.

In this work, we introduce a novel probabilistic approach for registration and analysis of transcriptome images and immunostaining images. The approach is grounded in a Bayesian framework and uses particle filters to determine the transformation between the images by jointly exploiting the information in the two channels. Both intensity information and image features are taken into account. We applied our approach to two-channel synthetic data as well as real tran-

scriptome images and immunostaining microscopy images of the mouse brain. It turns out that our approach accurately registers the multi-modal images and yields better results than a state-of-the-art method.

## 2. METHODOLOGY

Our probabilistic registration approach consists of three main steps: (i) Gene expression matrix visualization (ii) spots detection and joint registration, and (iii) Voronoi-based cell segmentation.

### 2.1. Gene expression matrix visualization

The gene expression matrix is visualized by plotting white dots on the black canvas, a rectangular area intended for drawing dots. The x and y coordinates represent the horizontal and vertical positions of a pixel, respectively. In addition, the unique molecular identifier (UMI) count value of each position is used as the intensity value of the dot.

In order to emulate the real distance between dots, we adjust the dot size according to the relation between dot size and canvas image size. Let $D_{circle}$ be the diameter of a dot, $w$ the width of a canvas image (unit: inch), $h$ the horizontal coordinate range of the gene expression matrix, and $f_{mag}$ the factor for dot magnification. The size of each dot $s_{dot}$ then be calculated by:

$$s_{dot} = D_{circle}^2 = (72 \times \frac{w}{h} \times f_{mag})^2. \tag{1}$$

### 2.2. Probabilistic approach for registration

Our target is to study the relationship between the spatial cell structure in the immunostaining image and the corresponding gene expression distribution in the gene expression matrix image. The goal of registration is to assign $N_g$ gene expression spots to $N_c$ cells. Such assignment can be represented as a non-negative assignment matrix $\omega$ with elelments $\omega_{n_g}^{n_c}$ that denote the strength of gene expression for a spot $n_g$ within a cell $n_c$ (using a binary assignment $\omega \in \{0,1\}^{N_g \times N_c}$). Some nodes may be assigned to no cells. Within a Bayesian framework, this task can be formulated by estimating the posterior probability density $p(\omega \mid I^i, I^g)$, where $I^i$ is the immunostaining image and $I^g$ is the gene expression matrix image. We denote the positions of all detected spots in the immunostaining image by $\boldsymbol{Y}_{1:N_c}^i$ and denote the positions of all detected spots in gene expression image by $\boldsymbol{Y}_{1:N_g}^g$. To detect and localize spots, we use an approach based on the spot-enhancing filter [9, 10]. Since all cells are located within the same plane in our application, the transformation between the multi-modal images can be represented by a homography $\boldsymbol{H}$. Since $\boldsymbol{Y}_{1:N_c}^i$ and $\boldsymbol{Y}_{1:N_g}^g$ are conditionally independent of $I^i$ and $I^g$, by using Bayes' theorem, we can write

$$\begin{aligned} &p(\boldsymbol{Y}_{1:N_c}^i, \boldsymbol{Y}_{1:N_g}^g, \boldsymbol{H} \mid I^i, I^g) = \\ &p(\boldsymbol{H} \mid I^i, I^g, \boldsymbol{Y}_{1:N_c}^i, \boldsymbol{Y}_{1:N_g}^g) p(\boldsymbol{Y}_{1:N_c}^i \mid I^i) p(\boldsymbol{Y}_{1:N_g}^g \mid I^g). \end{aligned} \tag{2}$$

In our work, the transformation matrix is represented by

$$\boldsymbol{H}(\boldsymbol{x}) = \begin{pmatrix} s_x \cos(\theta) & s_x \sin(\theta) & t_x \\ -s_y \sin(\theta) & s_y \cos(\theta) & t_y \\ 0 & 0 & 1 \end{pmatrix}. \tag{3}$$

To determine the homography $\boldsymbol{H}$, we need to estimate the $5D$ parameter vector $\boldsymbol{x} = (s_x, s_y, \theta, t_x, t_y)$ with rotation angle $\theta$, scaling $s_x, s_y$, and translation $t_x, t_y$. As similarity metric between corresponding images we suggest using a combination of mutual information (MI) and the point set distance. The metric is maximized to align the multi-modal images.

Let $\mathrm{MI}\left(I^i, \boldsymbol{H}(\boldsymbol{x}) I^g\right)$ be the mutual information of $I^n$ and $\boldsymbol{H}(\boldsymbol{x}) I^g$, and $\mathrm{D}(\boldsymbol{Y}^i, \boldsymbol{H}(\boldsymbol{x}) \boldsymbol{Y}^g)$ be the sum of distances between points from $\boldsymbol{Y}^i$ and $\boldsymbol{H}(\boldsymbol{x}) \boldsymbol{Y}^g$. We search the optimal parameter vector $x^*$ by maximizing the following likelihood function

$$\begin{aligned} &\arg\max_{\boldsymbol{x}} p(\mathrm{MI}(I^i, \boldsymbol{H}(\boldsymbol{x}) I^g)) p(\mathrm{D}(\boldsymbol{Y}^i, \boldsymbol{H}(\boldsymbol{x}) \boldsymbol{Y}^g)) = \\ &\arg\max_{\boldsymbol{x}} \exp\{\frac{\mathrm{MI}(I^i, \boldsymbol{H}(\boldsymbol{x}) \boldsymbol{Y}^g))}{2\sigma_{MI}^2}\} \exp\{\frac{\mathrm{D}(\boldsymbol{Y}^i, \boldsymbol{H}(\boldsymbol{x}) \boldsymbol{Y}^g))}{(-1) * 2\sigma_D^2}\}, \end{aligned} \tag{4}$$

where $\sigma_{MI}$ is the standard deviation of MI and $\sigma_D$ is the standard deviation of the point set distance.

Naively, we could exhaustively search the whole parameter space to find the maximum likelihood so that the best alignment between the two images can be obtained. However, this is time consuming. Here, we suggest using particle filters to efficiently determine the optimal $\boldsymbol{x}^*$ in Eq. (4), given a random initial $\boldsymbol{x}$.

Furthermore, we can estimate $\omega_{n_g}^{n_c}$ for each gene expression spot $n_g$ at each cell $n_c$ for a given observations $\boldsymbol{Y}_{n_c}^i$ and $\boldsymbol{Y}_{n_g}^g$. Voronoi tessellation [11] can be used to find a rough boundary of each cell.

## 3. EXPERIMENTAL RESULTS

We compared our registration method with the state-of-the-art registration method [8] using synthetic as well as real immunostaining images and gene expression matrix images. For synthetic data, we generated immunostaining images ($500 \times 500$ pixels) were imaged on using SimuCell [12] and randomly determined transformations as GT transformations. For real data of the mouse brain ($964 \times 964$ pixels, pixel size $0.65 \times 0.65 \mu\mathrm{m}^2$), the GT transformation was obtained by manual alignment.

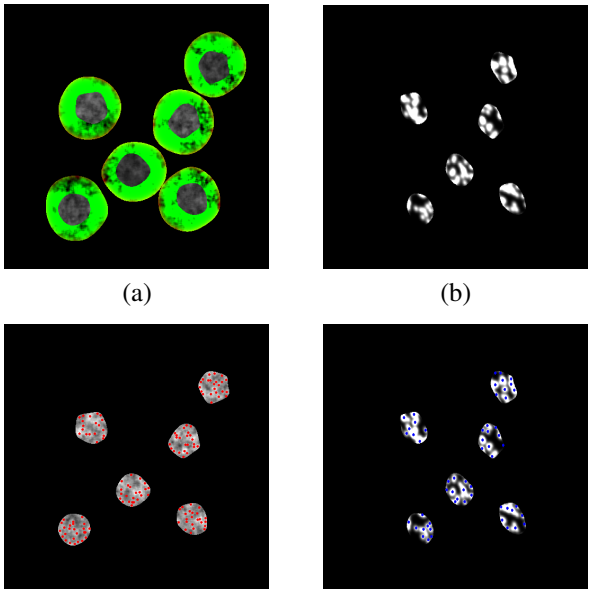


**Fig. 2**. Results of our approach for synthetic data: (a) Immunostaining image, (b) gene expression matrix image, (c) detected particles in immunostaining image (red), and (d) detected particles in gene expression matrix image (blue).

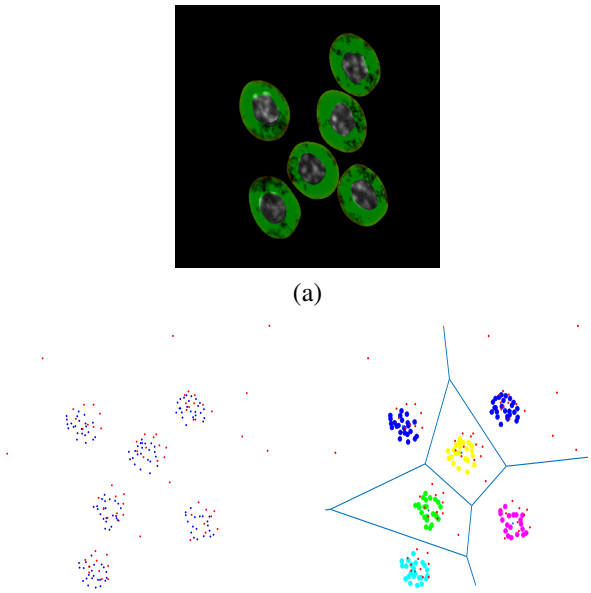


**Fig. 3**. Result of our approach for synthetic data with noise: (a) Overlay of registered immunostaining image and gene expression matrix image, (b) overlay of detected spots in both images after registration (red: detected spots in immunostaining image, blue: detected spots in gene expression matrix image), (c) cell segmentation of each cell region by Voronoi tesselation.

The registration result was quantified by the registration error (TRE), which is the average distance between the positions determined by the computed transformation parameters and the GT parameters. We used six points to compute the TRE and determined the average position error in the $x$ and $y$ directions of the aligned points. Let $\boldsymbol{H}(\boldsymbol{x}^*)$ be the computed transformation matrix and $\boldsymbol{p}_q, q \in \{1, \cdots, 6\}$ be the chosen points, then the TRE is computed by

$$\begin{aligned} TRE_x &= \tfrac{1}{6}\textstyle\sum_{q=1}^{6} d_x\left(\boldsymbol{p}_q^i, \boldsymbol{H}(\boldsymbol{x}^*)\boldsymbol{p}_q^g\right) \\ TRE_y &= \tfrac{1}{6}\textstyle\sum_{q=1}^{6} d_y\left(\boldsymbol{p}_q^i, \boldsymbol{H}(\boldsymbol{x}^*)\boldsymbol{p}_q^g\right) \end{aligned} \tag{5}$$

where $d_x, d_y$ denote the distance between two corresponding points in $x$ and $y$ direction. $\boldsymbol{p}_q^i$, $\boldsymbol{p}_q^g$ are two corresponding points in the immunostaining image and the gene expression matrix image.

For our probabilistic registration approach, we used 50 random samples and 10 time steps for the particle filter to the transformation matrix in Eq. (3).

| Image | #Cells | Method [8] | | Ours | |
|---|---|---|---|---|---|
| | | $TRE_x$ | $TRE_y$ | $TRE_x$ | $TRE_y$ |
| 1 | 5 | 8.32 | 15.65 | 2.27 | 9.78 |
| 2 | 20 | 15.14 | 17.37 | 2.88 | 13.37 |
| 3 | 80 | 6.84 | 20.74 | 3.29 | 15.38 |
| 4 | 320 | 12.89 | 23.84 | 5.17 | 17.16 |
| *average* | 106 | 10.80 | 19.40 | 3.40 | 13.92 |

**Table 1**. Target registration error for synthetic images.

| Images | #Cells | Method [8] | | Ours | |
|---|---|---|---|---|---|
| | | $TRE_x$ | $TRE_y$ | $TRE_x$ | $TRE_y$ |
| 1 | 256 | 22.68 | 23.17 | 12.21 | 16.56 |
| 2 | 153 | 18.14 | 15.37 | 8.44 | 15.42 |
| 3 | 175 | 22.84 | 27.74 | 10.29 | 13.38 |
| 4 | 208 | 23.89 | 22.84 | 10.17 | 14.16 |
| *average* | 198 | 21.89 | 22.28 | 10.28 | 14.88 |

**Table 2**. Target registration error for real images.

Table 1 and Table 2 provide the TRE of our registration approach and the method in [8] for four pairs of synthetic im-

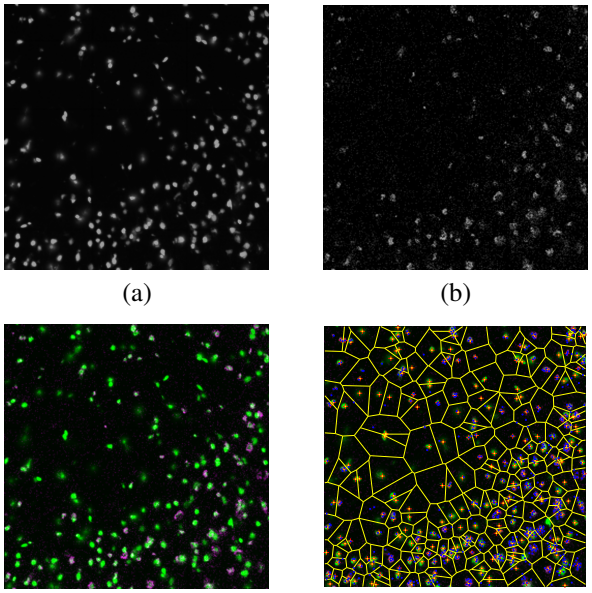


**Fig. 4**. Results of our approach for real data (image section): (a) Immunostaining image, (b) gene expression matrix image, (c) overlay of registered images, (d) cell segmentation result (red cross points: detected immunostaining image nucleus midpoints, blue points: detected gene expression matrix spots, and yellow lines: estimated boundaries of cells).

ages and 4 pairs of real images. For all image pairs, the TRE of our approach is much lower than that of method [8]. Thus, that our approach is much more accurate than the previous method for challenging data.

## 4. CONCLUSIONS

We have presented a probabilistic approach for multi-modal registration of transcriptomics image data. Our approach estimates the transformation matrix for the microscopy image and gene expression matrix. The method exploits information from two channels simultaneously, and the transformation matrix is adjusted iteratively. Our approach has been successfully applied to synthetic data and real spatial transcriptomics data of mouse brains, and we found that the method yields accurate results.

## 5. ACKNOWLEDGEMENTS

This work was supported by the BGI-Research and the Institute of Neuroscience (ION) of the Chinese Academy of Sciences. In addition, The authors gratefully acknowledge Prof Mu-ming Poo, Qing Xie, and Ao Chen for providing mouse brain spatial transcriptomics data and many helpful discussions during development.

## 6. REFERENCES

[1] A. Rao, D. Barkley, G. S. França, and I. Yanai, "Exploring tissue architecture using spatial transcriptomics," *Nature*, vol. 596, no. 7871, pp. 211–220, 2021.

[2] A. Chen, S. Liao, K. Ma, L. Wu, Y. Lai, J. Yang, W. Li, J. Xu, S. Hao, X. Chen, et al., "Large field of view-spatially resolved transcriptomics at nanoscale resolution," *bioRxiv*, 2021.

[3] C.-S. Cho, J. Xi, Y. Si, S.-R. Park, J.-E. Hsu, M. Kim, G. Jun, H. M. Kang, and J. H. Lee, "Microscopic examination of spatial transcriptome using seq-scope," *Cell*, 2021.

[4] N. Yoosuf, J. F. Navarro, F. Salmén, P. L. Ståhl, and C. O. Daub, "Identification and transfer of spatial transcriptomics signatures for cancer diagnosis," *Breast Cancer Research*, vol. 22, no. 1, pp. 1–10, 2020.

[5] M. Saiselet, J. Rodrigues-Vitória, A. Tourneur, L. Craciun, A. Spinette, D. Larsimont, G. Andry, J. Lundeberg, C. Maenhaut, and V. Detours, "Transcriptional output, cell-type densities, and normalization in spatial transcriptomics," *Journal of Molecular Cell Biology*, vol. 12, no. 11, pp. 906–908, 2020.

[6] W.-T. Chen, A. Lu, K. Craessaerts, B. Pavie, C. S. Frigerio, N. Corthout, X. Qian, J. Laláková, M. Kühnemund, I. Voytyuk, et al., "Spatial transcriptomics and in situ sequencing to study Alzheimer's disease," *Cell*, vol. 182, no. 4, pp. 976–991, 2020.

[7] X. Papademetris, A. P. Jackowski, R. T. Schultz, L. H. Staib, and J. S. Duncan, "Integrated intensity and point-feature nonrigid registration," in *Proc. MICCAI 2004*. Springer, 2004, pp. 763–770.

[8] R. Chen, A. B. Das, and L. R. Varshney, "Registration for image-based transcriptomics: Parametric signal features and multivariate information measures," in *Proc. 2019 53rd Annual Conference on Information Sciences and Systems (CISS)*. IEEE, 2019, pp. 1–6.

[9] D. Sage, F. R. Neumann, F. Hediger, S. M. Gasser, and M. Unser, "Automatic tracking of individual fluorescence particles: application to the study of chromosome dynamics," *IEEE Transactions on Image Processing*, vol. 14, no. 9, pp. 1372–1383, 2005.

[10] Y. Qiang, J. Y. Lee, R. Bartenschlager, and K. Rohr, "Colocalization analysis and particle tracking in multi-channel fluorescence microscopy images," in *Proc. ISBI 2017*. IEEE, 2017, pp. 646–649.

[11] M. Bock, A. K. Tyagi, J.-U. Kreft, and W. Alt, "Generalized Voronoi tessellation as a model of two-dimensional cell tissue dynamics," *Bulletin of Mathematical Biology*, vol. 72, no. 7, pp. 1696–1731, 2010.

[12] S. Rajaram, B. Pavie, N. E. Hac, S. J. Altschuler, and L. F. Wu, "Simucell: a flexible framework for creating synthetic microscopy images," *Nature Methods*, vol. 9, no. 7, pp. 634–635, 2012.